Mechanisms of tubular volume retention in immune-mediated glomerulonephritis

Juliane Gadau[1,5], Harm Peters[2,5], Christian Kastner[1], Hartmut Kühn[3], Melina Nieminen-Kelhä[2], Dmytro Khadzhynov[2], Stephanie Krämer[2], Hayo Castrop[4], Sebastian Bachmann[1] and Franziska Theilig[1]

[1]Institute of Anatomy, Charité Universitätsmedizin, Berlin, Germany; [2]Department of Nephrology, Charité Universitätsmedizin, Berlin, Germany; [3]Department of Biochemistry and Biophysics, Charité Universitätsmedizin, Berlin, Germany and [4]Institute of Physiology, University Regensburg, Regensburg, Germany

Glomerulonephritis is characterized by hematuria, proteinuria, hypertension, and edema, but the mechanisms contributing to volume disorders are controversial. Here we used the rat anti-Thy1 model of mesangioproliferative glomerulonephritis to test the hypothesis that disturbed salt and water homeostasis is based on tubular epithelial changes that cause salt retention. In this model there was an early onset of pronounced proteinuria and lipiduria associated with reduced fractional sodium excretion and a lowering of the renin–angiotensin–aldosterone system. The glomerular filtration rate and creatinine clearance were decreased on day 6. There was a reduced abundance of the major salt and water transport proteins on the proximal tubular brush border membrane and which paralleled cellular protein overload, enhanced membrane cholesterol uptake and cytoskeletal changes. Alterations in thick ascending limb were moderate. Changes in the collecting ducts were characterized by an enhanced abundance and increased subunit cleavage of the epithelial sodium channel, both events consistent with increased sodium reabsorption. We suggest that irrespective of the proximal tubular changes, altered collecting duct sodium reabsorption may be crucial for volume retention in acute glomerulonephritis. We suggest that enhanced proteolytic cleavage of ion transporter subunits might be a novel mechanism of channel activation in glomerular diseases. Whether these proteases are filtered or locally secreted awaits determination.

Kidney International (2009) **75,** 699–710; doi:10.1038/ki.2008.649; published online 4 February 2009

KEYWORDS: collecting duct; ENaC; lipids; proteases; proteinuria; proximal tubule

Correspondence: *Franziska Theilig or Sebastian Bachmann, Charité – Universitätsmedizin Berlin, Institut für Vegetative Anatomie, Philippstr. 12, 10115 Berlin, Germany.*
E-mails: franziska.theilig@charite.de or sbachm@charite.de

[5]These authors contributed equally to this study.

Received 1 April 2008; revised 21 October 2008; accepted 4 November 2008; published online 4 February 2009

Proteinuria is a common feature of acute and chronic nephropathies and a key predictor of declining glomerular filtration rate (GFR) in patients. Irrespective of the cause, proteinuria has been viewed as an independent factor for tubulointerstitial damage induced by direct toxicity of filtered protein,[1,2] although this concept has been questioned by others.[3–5] As a relevant systemic aspect, the substantial amounts of protein passing through the damaged filter to be lost in the urine cause symptoms such as interstitial edema, renal salt and water retention, and hypertension.[6,7] The potential causes for these disorders have been partly elucidated in models of the nephrotic syndrome (NS), but few studies have so far addressed their pathophysiological origins in glomerulonephritis (GN) and consequent nephritic syndrome.

Salt retention in the NS has traditionally been explained by the hypovolemia concept, implying decreased oncotic pressure following proteinuria, loss of fluid into the interstitium, and activation of the renin–angiotensin–aldosterone system.[8,9] Meanwhile it has been claimed that the vascular volume in NS often remains unchanged along with the absence of blood pressure and renin–angiotensin–aldosterone system effects.[10,11] It has become accepted that primary tubular salt retention may *per se* produce a substantial systemic volume expansion in proteinuric nephrosis ('circulatory overfilling').[6,12]

Potential sites of sodium retention along the renal tubule have mostly been studied in the puromycin aminonucleoside rat model of NS, mimicking minimal change glomerular disease in human pathology.[7,9,13] Retention has been attributed to changes in the Na^+/H^+ exchanger-3 (NHE3) as the main pathway for Na reabsorption in the proximal tubule.[13–15] Generally, protein overload may impair proximal tubule structure and consequent handling of membrane proteins. Cytoskeletal changes may interfere with trafficking of transporters and channels, and the effects of inflammatory and profibrotic cytokines have been implicated.[1–3,16–20] Epithelial function may further be hampered by filtered lipoproteins and tubular accumulation of cholesterol.[21,22] Variations in plasma membrane cholesterol content may therefore alter cell signaling events and influence the viability of proximal ion transporters.[23,24] In the distal nephron,

regulation of the Na^+-K^+-$2Cl^-$ cotransporter-2 (NKCC2) of thick ascending limb (TAL) of Henle's loop may be affected,[9] and accumulating evidence points to the collecting ducts as a crucial site of sodium retention.[25,26] Recent study has been focussed on the activation of the epithelial Na^+ channel (ENaC) in a renin–angiotensin–aldosterone system-independent way.[10,11,27,28] New perspectives have come from observations that ENaC subunits were cleaved by serine proteases, increasing the open probability of the channel.[29–31]

In human disease, NS and acute GN or the resulting nephritic syndrome may produce in part similar volume disorders, but clinical features such as hematuria, reduced GFR, hypertension, and a less pronounced proteinuria are characteristics of acute GN. The aim of this study was to analyze tubular causes for volume disorders in the anti-Thy1 rat model for immune-mediated acute GN.

RESULTS

Laboratory parameters and renal functional data

Generally, control rats and anti-Thy1 GN rats were observed during a 6-day period. As detailed in the 'Materials and Methods' section, three protocols were established to obtain laboratory parameters during the time course and at the final time point when kidneys were removed for analysis. On day 6, all anti-Thy1-treated rats had developed severe GN with marked proteinuria, whereas no changes were recorded in plasma protein and albumin levels, and signs of ascites were absent. Urinary protein excretion was markedly enhanced in anti-Thy1 GN, and so was albumin excretion (protocol (I); Table 1). Plasma creatinine levels were increased, whereas its renal clearance was decreased in anti-Thy1 GN rats at the final time point. Importantly, the 24-h urinary sodium excretion as well as the urinary sodium/creatinine was decreased. The fractional excretion of sodium (FE_{Na}) was not significantly altered owing to the decreased GFR. Urinary osmolality was significantly reduced, which may indicate a defect in urinary concentrating mechanism but may also be related to the overall decreased excretion of osmotically active molecules. Plasma cholesterol and triglyceride levels were significantly increased ($P<0.05$) along with much higher augmentations in urinary free cholesterol and cholesterol metabolite excretion, indicating hyperlipidemia and excessive lipiduria ($P<0.001$; Table 1). The kidney weight was increased in anti-Thy1 GN rats, suggesting a correlation with the known disease-related hypertrophy and/or hyperplasia of glomeruli and nephron epithelia.

Daily sodium intake and fecal sodium output did not differ between controls and anti-Thy1 GN rats evaluated according to protocol (II). In anti-Thy1 GN, daily urinary sodium output was significantly decreased from day 4 onward and remained low until the end of the experiment (Figure 1). Daily sodium balance was significantly increased from day 4 onward and remained positive until the last day. Proteinuria was maximally elevated on day 2 and remained high further on. To examine GFR during the time course of the experiment, inulin clearance was determined in controls and anti-Thy1 GN rats according to protocol (III) on days 2, 3, 4, and 6. Creatinine clearance and FE_{Na} were measured in parallel (Figure 1). Inulin clearance as well as 24-h creatinine clearance was not significantly different between anti-Thy1 GN and controls on days 2, 3, and 4, respectively, whereas on day 6, inulin and creatinine clearances were significantly reduced. FE_{Na} of anti-Thy1 GN rats was significantly reduced on days 2, 3, and 4, but had increased to control levels on day 6.

Table 1 | Clinical parameters and alterations in renal function

	Controls	Anti-Thy1 GN
General data		
Body weight (g)	264.88 ± 10.77	258.68 ± 17.10
Kidney weight (g)	2.19 ± 0.17	2.85 ± 0.55*
Mean systolic blood pressure (mm Hg)	122.33 ± 3.10	122.32 ± 3.96
Water uptake (ml)	34.60 ± 10.69	36.90 ± 14.08
Urinary volume (ml)	17.19 ± 4.17	20.01 ± 13.25
Plasma analysis		
Na^+ (mmol/l)	152.20 ± 0.42	153.20 ± 0.38
K^+ (mmol/l)	5.22 ± 0.42	4.32 ± 0.38
Cl^- (mmol/l)	101.60 ± 2.61	105.40 ± 5.59
Protein (g per 100 ml)	4.96 ± 0.40	4.60 ± 0.28
Albumin (g per 100 ml)	2.42 ± 0.64	2.40 ± 0.48
Creatinine (mg per 100 ml)	0.20 ± 0.05	0.35 ± 0.08*
Cholesterol (mg per 100 ml)	51.36 ± 10.51	82.50 ± 22.47*
Triglyceride (mg per 100 ml)	68.91 ± 24.97	135.75 ± 76.15*
Urea (mg per 100 ml)	31.60 ± 10.55	75.00 ± 15.70*
Renal function		
Creatinine-clearance GFR (μl/min per g body weight)	11.93 ± 2.89	6.88 ± 1.33*
Fractional Na^+ excretion (FE_{Na};%)	0.34 ± 0.12	0.37 ± 0.14
Urinary analysis		
Na^+ (mmol per 24 h)	2.16 ± 0.14	1.58 ± 0.23*
K^+ (mmol per 24 h)	4.94 ± 0.67	3.36 ± 0.22*
Cl^- (mmol per 24 h)	2.91 ± 0.22	2.04 ± 0.21*
Osmolality (mOsm per kg H_2O)	1640 ± 100	1040 ± 180*
Protein (mg per 24 h)	15.07 ± 5.86	156.13 ± 64.11†
Albumin (mg per 24 h)	0.19 ± 0.23	23.02 ± 6.45†
Creatinine (mg per 24 h)	9.47 ± 0.93	8.64 ± 1.00
Urea (mg per 24 h)	673.18 ± 136.64	490.55 ± 53.73
Free cholesterol (μg per 24 h)	7.53 ± 4.46	115.95 ± 49.11†
Cholesterol linoleate (μg per 24 h)	2.28 ± 2.28	393.15 ± 143.56†
Cholesterol arachidonate (μg per 24 h)	8.15 ± 6.42	1452.65 ± 788.87†

GFR, glomerular filtration rate; GN, glomerulonephritis.
Values are measured on the last day of the experiment (protocol I; day 6; means ± s.e.).
*$P<0.05$; †$P<0.005$; n=10.

Histopathology

Immunohistochemical staining for the C5b-9 membrane attack complex indicated complement deposition in the mesangium in anti-Thy1 GN compared with control (Figure 2a and b). Paraffin histology revealed glomerular hypertrophy, mesangiolysis, and formation of proteinaceous crescents within Bowman's space. Tubules focally displayed not only collapse or atrophy and cast formation, but also epithelial hypertrophy (Figure 2c and d). Periodic acid Schiff-positive deposits were detected in proximal tubule and medullary and

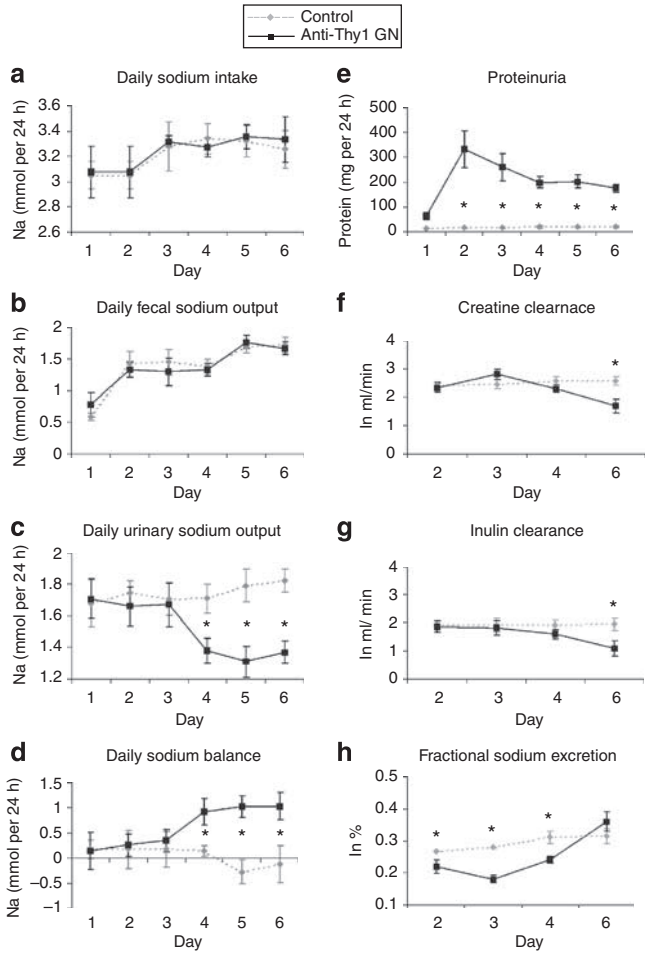

Figure 1 | Daily sodium metabolism, proteinuria, and renal function in anti-Thy1 GN. Rats had either received vehicle (control) or OX-7 for induction of anti-Thy1 GN. Days are numbered from 24 h after the injection onward. Panels show sodium handling, proteinuria, GFR, and FE_{Na} as obtained from collections in metabolic cages, blood sampling, and clearance measurements. Daily sodium intake and fecal sodium output show no differences between groups. Daily urinary sodium output in anti-Thy1 GN rats diverges from controls from day 4 onward, with parallel increases in sodium balance. Proteinuria in anti-Thy1 GN is raised from day 2 onward and remains strong throughout the experiment. GFR, as obtained by 24 h creatinine clearance and by inulin clearance, differs between groups on day 6. FE_{Na} is significantly decreased on days 2 and 4, but equals control levels on day 6. Panels **a**–**e** are from protocol (II) ($n = 12$), and **f**–**h** from protocol (III) ($n = 10$ on each time point); values are means ± s.e.; $^*P < 0.05$. GFR, glomerular filtration rate; GN, glomerulonephritis.

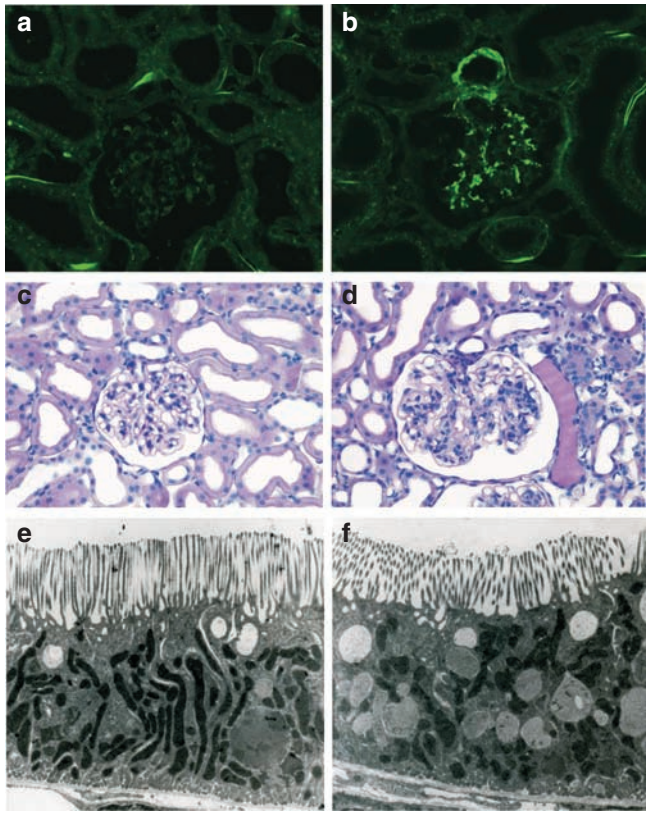

Figure 2 | Histopathology of anti-Thy1 GN. (**a** and **b**) Indirect immunofluorescence staining of C5b-9 membrane attack complex. Deposits of C5b-9 are visible in extra- and intraglomerular mesangium and occasionally at the juxtaglomerular apparatus in GN (**b**). (**c** and **d**) Periodic acid Schiff staining of kidney sections from control (**c**) and GN (**d**). Severe glomerular and mild tubulointerstitial changes are obvious in GN (**d**). (**e** and **f**) Fine structural evaluation of proximal tubule cells from control (**e**) and GN (**f**). A strong accumulation of secondary and tertiary lysosomes is observed in GN (**e**). (**a**–**d**) Magnification × 250; (**e** and **f**) magnification × 4600. GN, glomerulonephritis.

cortical TALs. Massive accumulations of lysosomes were identified in the proximal tubule (Figure 2e and f). Occasionally, loss of brush border membrane (BBM) was observed, and the abundances of villin as a major BBM component, and megalin, a protein involved in endocytosis, were reduced in anti-Thy1 GN (Figure 3a).

Expression of cortical and medullary transporter and channel proteins

Differential abundance of the major ion and water transporters and channels along the nephron and collecting duct system was evaluated by western blot. Proximal tubular aquaporin-1 (AQP1), NHE3, and Na^+-P_i cotransporter-IIa (NaPi-IIa) were quantified from BBM preparations. Densitometric evaluation of band intensities revealed reduced expression of these transporters in anti-Thy1-treated animals (Figures 3 and 4; Table 2). These data were confirmed by immunohistochemical staining showing reduced intensity of AQP1, NHE3, and NaPi-IIa in the BBM of anti-Thy1 GN rats (Figure 5). The abundances of AQP2, NHE3, NKCC2, Na^+-Cl^- cotransporter (NCC), αENaC, βENaC, γENaC, αNa^+,K^+-ATPase (αNKA), and βNKA were evaluated by western blots from cortical membrane fractions. Densitometric quantification revealed a significant upregulation of αNKA, αENaC, and γENaC expression (Figures 3 and 4; Table 2). For αENaC and γENaC, apart from the major mature bands at approximately 90 kDa, additional lower molecular weight bands were present at approximately 65 and 70 kDa, respectively, and for γENaC, a second additional band at 55 kDa was registered (Figure 3). These additional bands were

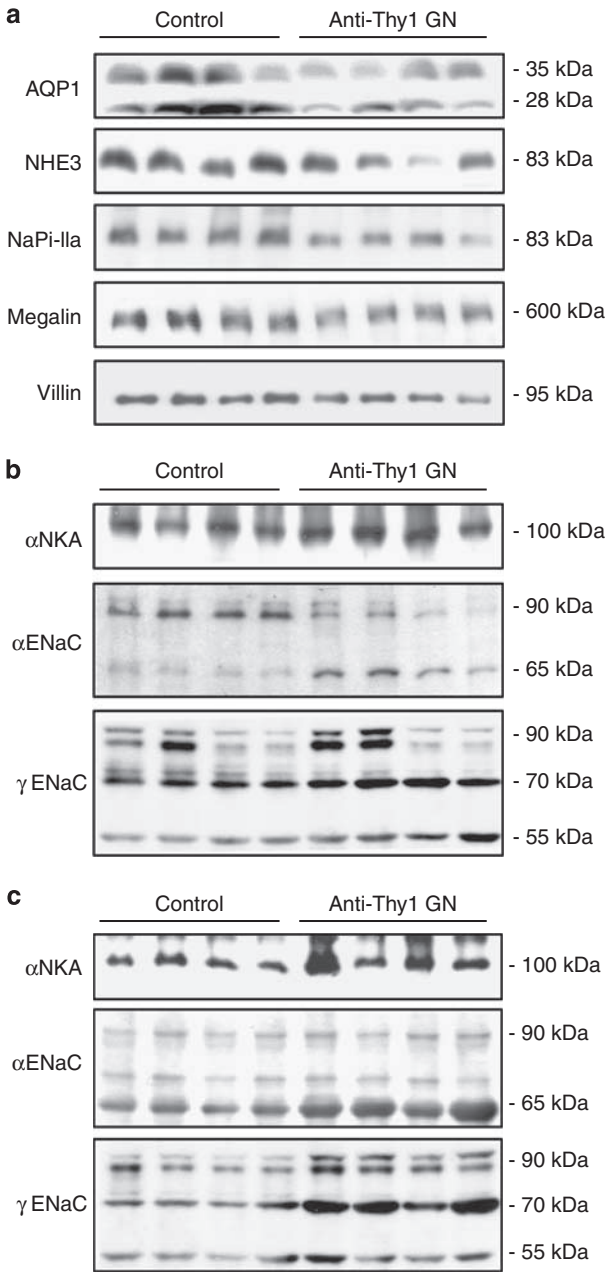

Figure 3 | Semiquantitative immunoblotting of transporter and channel proteins along the nephron. (**a**) Abundance of aquaporin-1 (AQP1), Na^+/H^+ exchanger-3 (NHE3), Na^+-P_i cotransporter-IIa (NaPi-IIa), megalin, and villin from brush border membrane fractions. (**b**) Abundance of α-subunit of Na^+,K^+-ATPase (NKA), and α- and γ-subunits of the epithelial Na^+-channel (ENaC) from cortical membrane fractions. (**c**) Abundance of αNKA and α- and γENaC from medullary membrane fractions. Apart from the major 90 kDa bands, additional lower molecular weight bands indicate increases in the cleaved forms of ENaC subunits in GN (**b** and **c**). The respective densitometric calculations are given in Table 2. GN, glomerulonephritis.

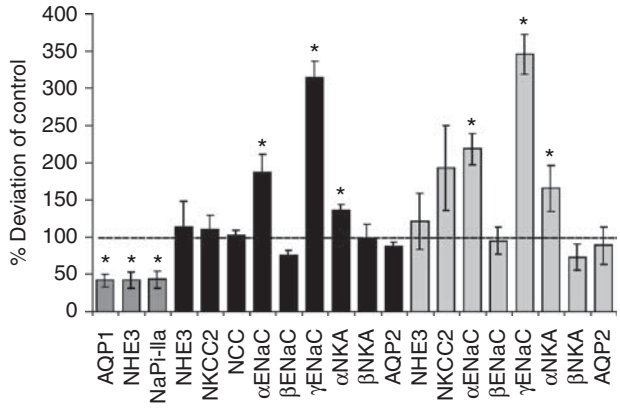

Figure 4 | Abundance of transporters and water channels along the nephron. A summary of densitometric values from immunoblots shown in Figure 3: aquaporin-1 (AQP1), Na^+/H^+ exchanger-3 (NHE3), Na^+-P_i cotransporter-IIa (NaPi-IIa), aquaporin-2 (AQP2), bumetanide-sensitive Na^+-K^+-$2Cl^-$ cotransporter-2 (NKCC2), thiazide-sensitive Na^+-Cl^- cotransporter (NCC), α-, β-, and γ-subunits of epithelial Na^+ channel (ENaC), and α- and β-subunits of Na^+,K^+-ATPase (NKA) from anti-Thy1 GN shown as percent deviations from controls, normalized to β-actin; brush border membrane fractions (dark gray columns), cortical membrane fractions (black columns), and medullary membrane fractions (gray columns). Values are means ± s.e.; $n = 10$; $^*P < 0.05$. GN, glomerulonephritis.

Table 2 | Western blot results of full-length and cleavage products of epithelial Na^+ channel α- and γ-subunit on days 2, 4, and 6

Cortical PM fraction, day 6	
αENaC (90 kDa)	35.37 ± 09.05 vs 100 ± 12.77
αENaC (65 kDa)	251.88 ± 36.84 vs 100 ± 13.12*
γENaC (90 kDa)	154.85 ± 27.22 vs 100 ± 16.28
γENaC (70 kDa)	220.90 ± 15.24 vs 100 ± 05.72*
γENaC (55 kDa)	139.14 ± 11.26 vs 100 ± 02.02*
Medullary PM fraction, day 6	
αENaC (90 kDa)	132.30 ± 03.11 vs 100 ± 03.78*
αENaC (65 kDa)	305.04 ± 37.19 vs 100 ± 11.49*
γENaC (90 kDa)	199.40 ± 25.70 vs 100 ± 09.79*
γENaC (70 kDa)	293.31 ± 28.76 vs 100 ± 07.93*
γENaC (55 kDa)	124.16 ± 13.71 vs 100 ± 02.02

Abbreviation: ENaC, epithelial Na^+ channel.
Values are densitometric intensity levels normalized for β-actin (means ± s.e.).
$^*P < 0.05$; n=5 per group.

strongly increased in anti-Thy1 GN, suggesting a selective cleavage of ENaC subunits under the proteinuric condition. The mature ENaC subunits in the 90 kDa range typically appeared as double bands, possibly owing to different glycosylation levels; they did not dissociate in GN and were therefore evaluated together. In contrast, abundances of AQP2, NHE3, NKCC2, NCC, βENaC, and βNKA were not significantly altered in anti-Thy1 GN (Figures 3 and 4; Table 2). Immunostaining for αNKA showed significant increases in basolateral staining along the entire cortical nephron and collecting duct system (Figure 6a and b). Signals for αENaC and γENaC showed an apical shift of signals in connecting tubule and collecting duct principal cells (Figure 6c–f). Medullary membrane preparations revealed analogous changes as found in the cortex, with αNKA, αENaC, and γENaC expression significantly increased as determined by western blotting and densitometric evaluation; increases in

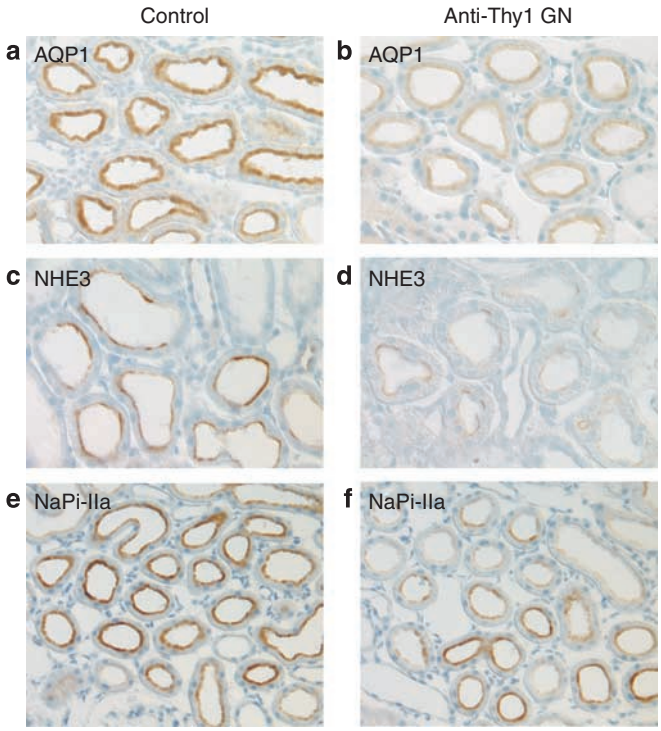

Figure 5 | Immunohistochemical staining of altered proximal tubular transport proteins: controls (left panels) and anti-Thy1 GN (right panels). (**a** and **b**) proximal tubular aquaporin-1 (AQP1); (**c** and **d**) proximal tubular Na^+/H^+ exchanger-3 (NHE3); (**e** and **f**) proximal tubular Na^+-P_i cotransporter-IIa (NaPi-IIa). Expression of AQP1, NHE3, and NaPi-IIa is strongly reduced in anti-Thy1 GN. (**a**–**d**) Magnification $\times$ 200; (**e** and **f**) magnification $\times$ 150. GN, glomerulonephritis.

αENaC and γENaC abundance were higher than in the cortex and also included the selective enhancements of the additional lower molecular weight bands in anti-Thy1 GN (Figures 3 and 4; Table 2). Immunostaining for outer medullary αNKA showed significant increases in basolateral staining along the proximal tubules and, more intensely, in collecting ducts (Figure 6g and h). Inner medullary collecting ducts showed enhanced αNKA staining in anti-Thy1 GN as well. As in cortex, signals for αENaC and γENaC showed apical signal increases in the collecting ducts (Figure 6i–l). During the time course of the experiments, increases in αNKA and selectively in the smaller αENaC and γENaC bands were also registered in whole kidney plasma membrane preparations from anti-Thy1 GN rats on days 2 and 4 (protocol (III); Table S1, Figure S1).

Anti-Thy1 GN-induced changes in renin, vasopressin, and 11βHSD-2

To assess whether changes in renal endocrine function could be related to alterations in epithelial transport under anti-Thy1 GN on day 6, we analyzed renal renin expression and plasma renin activity (PRA), plasma vasopressin, and the expression of 11β-hydroxysteroid dehydrogenase type-2 (11βHSD-2) as an essential tubular parameter mirroring the action of corticosteroids. Renal renin mRNA and protein

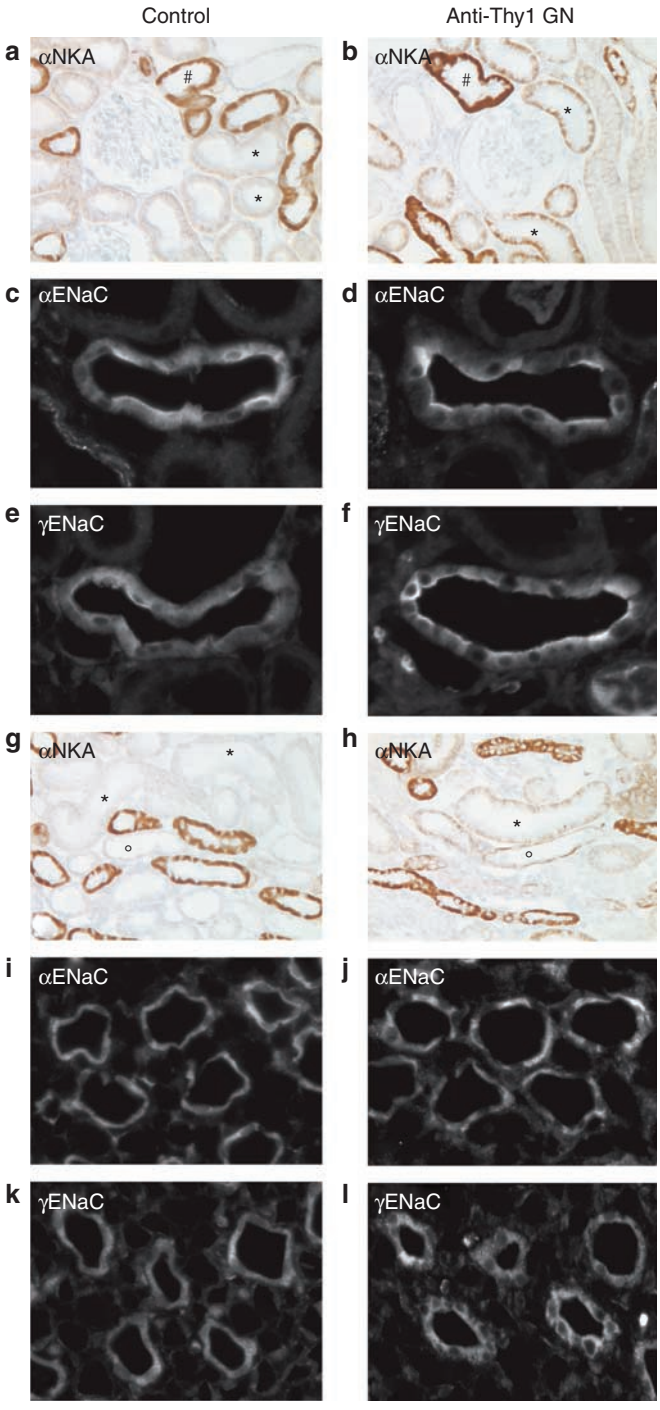

Figure 6 | Immunohistochemical staining of altered distal tubular transport proteins: controls (left panels) and anti-Thy1 GN (right panels). (**a** and **b**) α-subunit of Na^+,K^+-ATPase (αNKA), cortex with proximal segments (asterisk), and distal tubules (#); (**c** and **d**) α-subunit of the epithelial Na^+ channel (αENaC) in connecting tubule; (**e** and **f**) γ-subunit of ENaC (γENaC) in connecting tubule; (**g** and **h**) αNKA, outer medulla, with proximal segments (asterisk) and collecting ducts (◦); (**i** and **j**) αENaC in outer medullary collecting ducts; (**k** and **l**) γENaC in outer medullary collecting ducts. The abundance of αNKA is enhanced throughout, whereas ENaC signals are shifted toward the apical membrane in GN. (**a**, **b**, **g**, **h**) Magnification $\times$ 150; (**c**–**f** and **i**–**l**) magnification $\times$ 400. GN, glomerulonephritis.

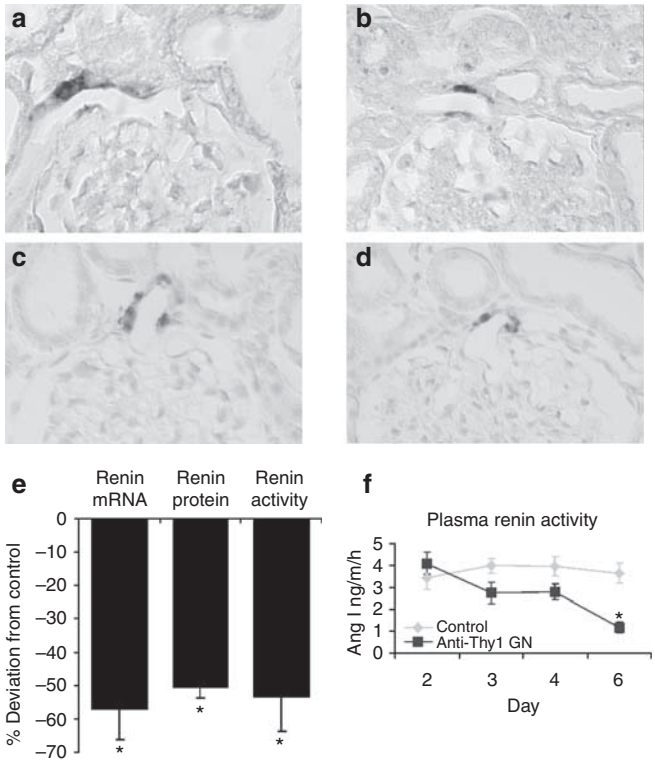

Figure 7 | Renin measurements. (**a**–**d**) representative images of histochemical abundances at the juxtaglomerular apparatus for renal renin mRNA (**a** and **b**) and renal immunoreactive renin (**c** and **d**) in controls (left panels) and anti-Thy1 GN (right panels) on day 6. Signals are reduced in GN. (**e**) Quantification of renal renin mRNA, renal immunoreactive renin, and plasma renin activity (PRA) on day 6. (**f**) Time course of PRA obtained on days 2, 3, 4, and 6. PRA in GN diverges significantly from controls on day 6. (**a**–**e**) From protocol (I) ($n = 10$); (**f**) is from protocol (III) ($n = 10$ on each time point). (**a**–**d**) Magnification $\times 400$; values are means ± s.e.; *$P < 0.05$. GN, glomerulonephritis.

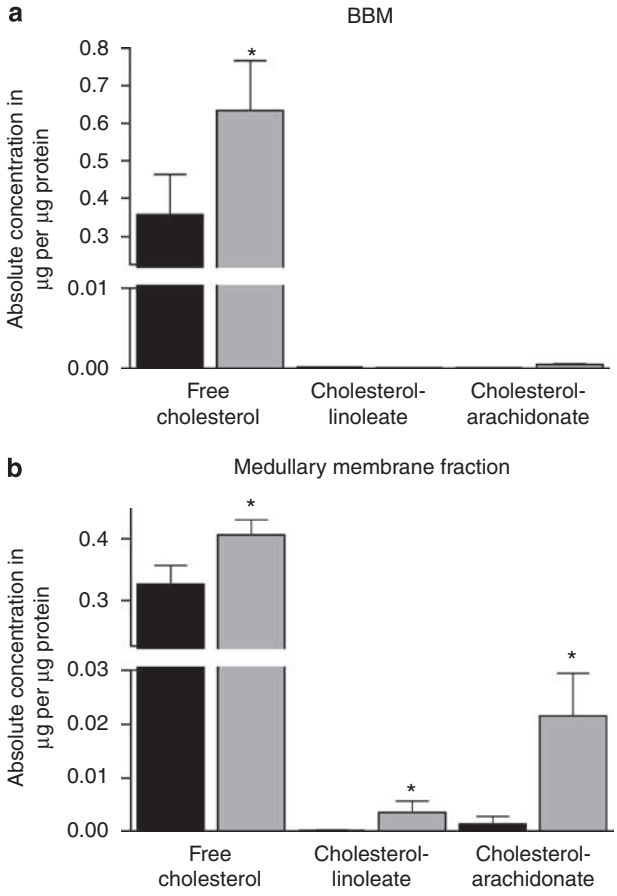

Figure 8 | Alterations in membrane lipid composition as obtained from HPLC analysis. Lipids had been extracted from membrane fractions. (**a** and **b**) Free cholesterol and esterified cholesterol (cholesterol linoleate and cholesterol arachidonate) in brush border membrane (BBM) (**a**) and medullary membrane fraction (**b**). Control (black columns); anti-Thy1GN group (gray columns). Values are means ± s.e.; $n = 10$; *$P < 0.05$. GN, glomerulonephritis; HPLC, high-performance liquid chromatography.

signals were significantly reduced in anti-Thy1 GN-treated rats compared with controls (0.56 ± 0.09 vs 1.00 ± 0.09 for renin mRNA and 0.50 ± 0.03 vs 1.00 ± 0.13 for renin immunoreactivity; $P < 0.05$; protocol (II); Figure 7). These results were paralleled by reduced PRA (0.53 ± 0.10 vs 1.00 ± 0.16; $P < 0.05$; protocol (II); Figure 7e). Plasma vasopressin levels in anti-Thy1 GN were not different from those in controls (22.80 vs 24.85 pg/ml). Likewise, the abundance of 11βHSD-2 expression as estimated by Western blots was not significantly altered on day 6 (1.05 ± 0.09 vs 1.00 ± 0.15 in the cortex and 1.01 ± 0.11 vs 1.00 ± 0.17 in the medulla). To assess the time course of PRA, plasma was sampled on days 2, 3, 4, and 6 (protocol (III)). Here, PRA in anti-Thy1 GN was numerically reduced on days 2, 3, and 4, but reached significance only on day 6 (Figure 7f).

Lipid composition of fractionated cell membranes

Effects of lipiduria (Table 1) on the absolute and esterified cholesterol content of BBM and medullary membrane fractions were studied by high-performance liquid chromatography. In both fractions, free cholesterol was augmented in the anti-Thy1 GN group compared with controls (0.63 ± 0.13 vs 0.36 ± 0.11 and 0.41 ± 0.02 vs 0.33 ± 0.03 µg per µg protein, respectively; $P < 0.05$; Figure 8a and b). In medullary membrane fractions, the abundance of esterified cholesterol showed particularly strong changes between groups.

Analysis of intracellular lipid accumulation

Intracellular lipid deposition was markedly increased in proximal tubule and TAL as revealed histochemically by the general lipid-staining agent, Sudan III (Figure 9b and d), whereas no signal was observed in control kidneys (Figure 9a and c). More specifically, intracellular cholesterol was identified by filipin staining, with signals localized to the cell membranes of epithelia in both groups (Figure 9e–h). Signal was enhanced in BBM and apical TAL cell membranes from anti-Thy1 GN kidneys (Figure 9f and h), and intracellular cholesterol deposits were identified in proximal and distal epithelia (Figure 9i and j).

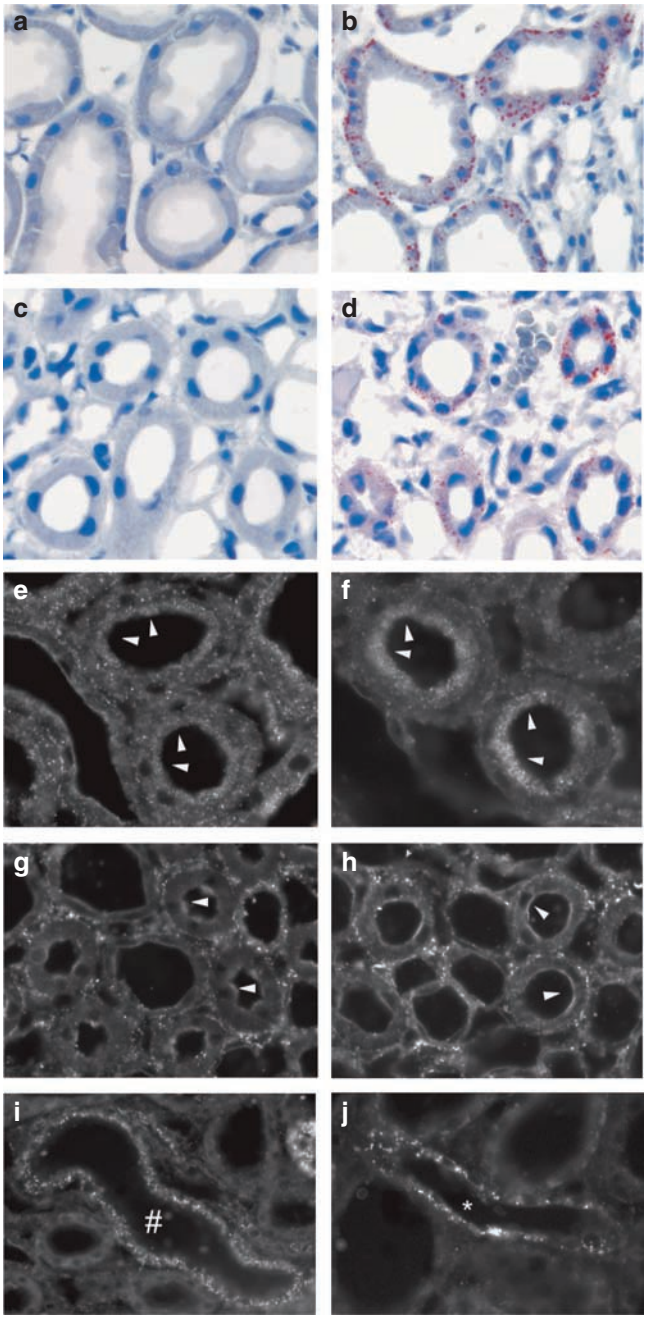

Figure 9 | Cellular lipid accumulation shown by histochemical lipid labeling in controls (left panels) and anti-Thy1 GN (right panels). (**a**–**d**) Sudan III general lipid staining; intracellular deposition of lipid droplets was restricted to proximal tubules (**b**) and medullary thick ascending limbs (TAL; **d**) of anti-Thy1 GN rats. (**e**–**j**) Fluorescent filipin staining of free cholesterol. In the cortex of controls, staining in brush border membrane of proximal tubules (arrowheads; **e** and **f**) and apical membrane of distal tubules (arrowheads; **g** and **h**) is enhanced in anti-Thy1 GN. Cholesterol droplets are occasionally observed focally in proximal tubules (#; **i**) and TAL (asterisk; **j**) of anti-Thy GN rats. (**a**–**j**) Magnification $\times$400. GN, glomerulonephritis.

Alterations in microtubule arrangements

Microtubules showed reduced α-tubulin immunostaining in proximal tubules of anti-Thy1 GN kidneys (Figure 10a and b). Microtubules of TAL were irregularly distributed and accumulated near the apical plasma membrane (Figure 10c and d).

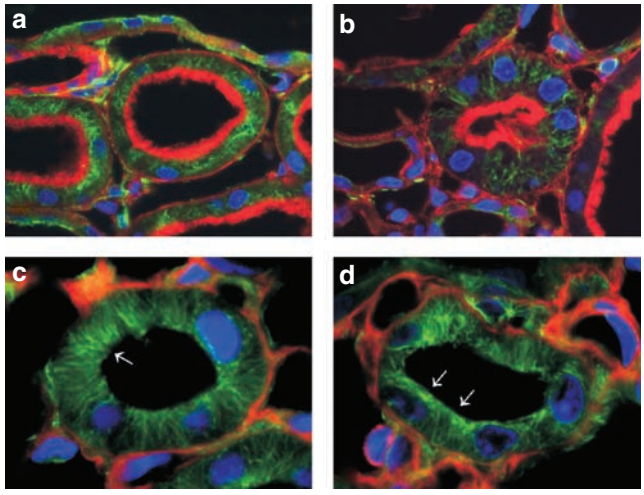

Figure 10 | Alterations of the cytoskeleton. (**a**–**d**) Triple staining of α-tubulin (green), f-actin (red), and nuclear staining with DAPI (blue) in proximal tubule (**a** and **b**) and medullary thick ascending limb profiles (TAL; **c** and **d**). Microtubules show diminished staining and reorientation in proximal epithelia of anti-Thy1 GN rats (**b**) compared with controls (**a**), and apical accumulation in patches, indicated by arrows, within TAL of anti-Thy1 GN (**d**) compared with controls (**c**). (**a** and **b**) Magnification $\times$400; (**c** and **d**) magnification $\times$600. DAPI, 4′,6-diamino-2-phenylindole; GN, glomerulonephritis; TAL, thick ascending limb.

DISCUSSION

This study contributes to the discussion whether primary, intrarenal-based salt and water retention or other systemic causes prevail in the volume disorders accompanying acute GN or the nephritic syndrome. To our knowledge, this study so far is the first approach to investigate mechanisms for primary sodium retention in immune-mediated GN. There is, however, overlap between our data and data on NS, which renders the present conclusions more broadly applicable among the two major glomerular syndromes. We have confirmed the known pathological and clinical landmarks of anti-Thy1 mesangioproliferative GN with glomerular C5b-9 accumulation, marked proteinuria and albuminuria, and reduced creatinine clearance.[4,19,32,33] In contrast to human GN, which can be associated with hypertension, anti-Thy1 GN in this study produced no changes in blood pressure. We could, however, present clear evidence for sodium retention as revealed by the markedly reduced absolute sodium excretion and reduced Fe_{Na}, suggesting a tendency toward increased systemic blood pressure, which may become more obvious with progression;[34] it was not until the final time point on day 6 that the difference in Fe_{Na} was blunted owing to a marked fall in GFR. Reduced renin angiotensin system parameters further agree with earlier data in anti-Thy1 GN.[35] Our study has revealed a number of segmental tubular epithelial changes, which together suggest that intrarenal

rather than systemic or circulatory factors may be involved in GN-related volume disorders.

With the bulk of sodium reabsorption occurring in the proximal tubule, this segment was considered to contribute to volume retention as reported from nephrotic rats.[13] However, the substantial reduction in BBM expression of three major proximal transport proteins in GN is opposed to enhanced sodium reabsorption at this site. Reduction of NHE3 as the principal representative of sodium entry reflects other similar findings in nephrotic rats;[27] along the same line, a micropuncture study in rats with unilateral nephrosis[25] showed reduced sodium reabsorption in proximal convoluted tubule and TAL. The reduced renin levels in anti-Thy1 GN, along with possibly reduced circulating angiotensin II levels, may as well be associated with retraction of NHE3 from the BBM and reduced sodium transport activity.[15,36]

The decrease in GFR in the anti-Thy1 GN group on day 6 suggests activation of tubulo-glomerular feedback. The drastic decrease in BBM AQP1 expression confirms this view, as AQP1-deficient mice losing up to 89% of proximal transcellular water passage had an activated feedback that prevented inadequate water and NaCl delivery to the distal nephron.[37,38] In keeping with this, the stabilization of sodium and water delivery to the postmacula region in NS was accomplished through an activated feedback.[25,26]

Patients with NS have multiple abnormalities in lipid metabolism, and fatty acids bound to albumin pass through the filter to reach the renal tubule in this condition.[21,39] Our results have shown an accumulation of cholesterol and its metabolites in proximal tubule BBM and medullary membranes along with the histochemical evidence for intracellular and membrane lipid accumulation. An excess of cellular fatty acids may cause cell dysfunction, and mice loaded with fatty acid and bovine serum albumin exhibited systemic water retention[40] so that altered transepithelial reabsorption of sodium and water in the present model may be related with these changes. As NaPi-IIa, NHE3, and possibly also AQP1 are lipid raft associated, trafficking or membrane association of these proteins may be impaired in an altered cholesterol environment.[23,24,41,42] This may as well be applied for distal epithelia in which NKA,[43] NKCC2,[44] and ENaC[45] were shown to be partially lipid raft dependent. The effects of lipid accumulation in the proximal tubule as compared with TAL may, however, be distinct with respect to activity of their membrane transporters. Accordingly, susceptibility to lipid accumulation of the proximal BBM and elaborate endosomal and recycling structures, and sites of complex shuttling routes to and from a transporter's site of action may not be the same as in the comparatively simple structures of the apical cell aspect in TAL. This may cause diverging effects regarding surface expression of the respective transporters.

Proteinuria has been classified as an independent risk factor in tubulo-interstitial disease, and much attention has been directed to inflammatory cytokines such as transforming growth factor-β in profibrotic signaling in response to protein overload.[1–3,19,20] Evidence thus points to transforming growth factor-β among the candidate products to determine proteinuria-related perturbation of the proximal tubule cells with regard to their apical transporters. The induction of transforming growth factor-β requires megalin/cubilin-dependent albumin uptake during protein overload, which has been demonstrated in megalin-deficient mouse models.[3] Among the consequences, major reductions in NHE3 activity and AQP1 abundance in another nephritic mouse model have been demonstrated.[46] Drastic cytoskeletal rearrangements have been shown earlier in proximal tubule cells exposed to transforming growth factor-β1, and their assumption of a fibroblastic nature was interpreted as epithelial–mesenchymal transition.[20,47] This and other studies, however, have provided little or no evidence for epithelial–mesenchymal transition.[3,5] The observed microtubular fragmentation rather agrees with the decreased surface expression of the transporters and thus with their diminished activity.[16,17,48] Microtubular changes were found also in TAL, but their adluminal appearance as well as the Western blot data on NKCC2 abundance was quite variable in our model, which agrees with the absence of clear changes in plasma vasopressin levels. Data on NKCC2 abundance in NS have been controversial as well.[49,50]

We have shown substantially enhanced expression of the α- and γ-subunits of ENaC, which is in keeping with our earlier study stating that the crucial site of sodium retention in proteinuric nephropathy lies beyond the distal convoluted tubule.[9,25–27] Amiloride, a diuretic that blocks ENaC-mediated sodium uptake, was consequently effective to restore sodium balance in cortical collecting duct (CCD) from kidneys with NS in an aldosterone-independent manner,[7,10,28] which agrees with the present lack of changes in 11βHSD-2, an enzyme mirroring the action of corticosteroids and their possible effects on NKA.[10,51,52] The rate-limiting role of ENaC has, however, also been questioned by some, stating that primary, aldosterone-independent induction of NKA may represent a sufficient mechanism for salt retention at the CCD in NS.[10,14] Conversely, increases in the abundance or shifts in the electrophoretic patterns of ENaC subunits may as well be viewed from the point that a related rise in intracellular sodium concentration *per se* can raise the activity of NKA.[53]

In this respect, the selective enhancements of the smaller 65 kDa band for the α-subunit and approximately 70 and 55 kDa bands for the γ-subunit in anti-Thy1 GN suggest that these electrophoretic shifts were related to enzymatic cleavage of the subunits, which partly would agree with published evidence on the size of cleaved ENaC products.[30,31,54,55] It has been well established that cleavage of ENaC subunits by proteases may lead to an activation of the channel. This mechanism has been illustrated by the original observation that amiloride-sensitive sodium currents had increased in response to extracellular serine protease,[54] and exogenously added trypsin or elastase as well as resident channel-activating proteases were later shown to have similar

effects.[29,31,55] Along the same line, proteases obtained from urines of nephrotic rats, such as the serine protease plasmin, were shown to activate ENaC.[30]

The origin of the 65 kDa αENaC band is not clear, as available data suggest that this molecular weight level is the result of endogenous cleavage.[55] Selective upregulation of the approximately 70 kDa-sized γENaC band, however, may well agree with published data on exogenous proteases generating a 67 kDa product.[55,56] The 55 kDa γENaC band has been mentioned earlier in the context of glycosylation so that it is unclear whether its selective increase in the medullary membrane fractions in the context of proteinuria is caused by proteolytic cleavage or deglycosylation, and whether this is related to an altered channel activity.[57] Together, ENaC cleavage products were elevated from early on during the time course of the study; already the initial increase in proteinuria on day 2 was accompanied by the selective rise in cleavage products along with elevated NKA abundance and reduced FENa; their causal links, however, remain to be established in future studies.

In sum, our study has identified renal changes in anti-Thy1 GN, which may be relevant to volume retention, hypertension, and edema formation in human nephritic syndrome. Our model shares some similarities with data obtained from nephrotic animal and cell models suggesting that altered filtrate composition and its tubular handling are the common denominators in renal-based phenotypic changes and antinatriuresis. In spite of marked alterations in proximal tubular BBM transporters, likely to be caused by the protein and lipid overload, our data support the notion that volume retention in acute GN, similar to NS, is focussed on sodium transport in the collecting ducts. Results are consistent with an otherwise established concept that proteolytic cleavage may activate ENaC subunits. Filtered plasma proteases could thereby facilitate apical sodium entry and cause volume retention in glomerular proteinuric syndromes.

MATERIALS AND METHODS

Animals and experimental protocol

Male Wistar rats ($n = 116$) weighing between 180 and 200 g were obtained from Charles River (Sulzfeld, Germany). Anti-Thy1 GN was induced by an intravenous injection of monoclonal antibody to OX-7 (1 mg per kg body weight in phosphate-buffered saline (PBS); pH 7.5) or vehicle (PBS).[19] Three sets of experiments (protocols I–III) were performed. Protocol (I): controls and anti-Thy1 GN rats (total $n = 24$) were used for the evaluation of histochemical, biochemical, and standard clinical parameters; rats were kept in normal cages during 6 days after the injections. They had unrestricted access to standard laboratory chow and tap water. For urine collection, rats were placed in metabolic cages during the last 24 h of the experiment. On day 6, 12 rats were isoflurane anesthetized, blood was collected, and the kidneys removed for biochemical analysis; the other 12 rats were perfusion fixed. Protocol (II): to determine salt balance on a daily base, controls and anti-Thy1 GN rats (total $n = 12$) were kept in metabolic cages throughout the experiment starting 24 h before injection of anti-Thy1 antibody. On day 6, blood samples were obtained and the animals killed. Protocol (III): to determine GFR by inulin clearance, controls and anti-Thy1 GN rats (total $n = 80$) were analyzed on days 2, 3, 4, and 6 after the injections. Clinical parameters including PRA were determined in parallel. Kidneys were obtained on days 2 and 4 for additional biochemical analysis (total $n = 20$). Rats were pair fed in protocols (II) and (III). All experiments were conducted in accordance with the German law for the protection of animals (project accredited by Berlin Senate Administration of Health).

Urine, blood, food, and fecal analysis

Serum and urine electrolytes were determined by indirect ion-selective electrode measurements (Modular Analytics; Roche Diagnostics, Mannheim, Germany). Urine osmolality was measured with an osmometer (Gonotec, Berlin, Germany). Blood urea nitrogen was quantified enzymatically and serum creatinine concentration was measured by the kinetic Jaffé method using routine automated methods (Modular Analytics; Roche Diagnostics). Creatinine clearance and fractional sodium excretion were calculated using standard equations. Total protein and albumin concentrations in serum and urine as well as cholesterol and triglyceride levels in serum were measured using standardized autoanalyzer methods (Hitachi 747, Hitachi 911, and STA analyzers; kits from Roche Diagnostics). Urinary concentration of free cholesterol and cholesterol esters was determined from total urinary lipid extracts by high-performance liquid chromatography (Shimadzu SPD-M10AVP instrument). Cholesteryl benzoate and/or cholesteryl pelargonate were used as external standards. For sodium measurements from feces and food, these were dried at 105 °C until a constant weight was reached, dissolved in 0.7 mol/l HNO_3, homogenized, and placed on a shaking table. Finally, sodium concentrations were determined in the supernatant by flame photometry (AFM 5051; Eppendorf, Hamburg, Germany).

Inulin clearance measurements

To determine inulin clearance, rats were anesthetized with isoflurane. Femoral veins and ureters were cannulated with polyethylene catheters. After receiving 10 ml per kg body weight of 0.45% saline to replace fluid losses during surgery, rats were given a bolus of 1% inulin/PBS intravenously, followed by a 90-min infusion period of 1% inulin/PBS (0.9 ml/h) and a 2-h infusion period of 1% inulin/0.45% saline as described.[58] Blood was collected during the ensuing 30-min clearance period for the determination of inulin concentration. Urine and plasma concentrations of inulin were determined by a kit (D-Glucose/D-Fructose Kit; R-Biopharm AG, Darmstadt, Germany).

Perfusion fixation and tissue processing for immunohistochemical evaluation

Rats were anesthetized by an intraperitoneal injection of sodium pentobarbital (0.06 mg per g body weight). Kidneys were then perfused *in vivo* through the abdominal aorta using 3% Paraformaldehyde (PFA) dissolved in PBS. For cryostat sectioning, tissues were protected from freezing artifacts by 800 mOsm sucrose/PBS, shock-frozen in cooled isopropane, and stored at −80°C. Alternatively, tissues were post-fixed in 3% PFA/PBS, dehydrated, and standard paraffin embedded. For ultrastructural analysis, kidney specimens were post-fixed in 1.5% PFA/PBS containing 1.5% glutaraldehyde and 0.05% picric acid, rinsed, and stored in PBS until embedding in Epon (Serva, Heidelberg, Germany).

Tissue processing for immunoblotting

Fractionation of the proximal tubule BBM of kidney cortices was performed as described.[59] Enrichment of BBM was found to be unaffected by the anti-Thy1 treatment based on the fact that the ratios between BBM and total cortical homogenate in alkaline phosphatase and γ-glutamyltransferase activities in controls and anti-Thy1-GN rats were not different ($\times 5.7 \pm 0.6$ vs $\times 7.8 \pm 4.8$ and $\times 6.4 \pm 1.4$ vs $\times 7.6 \pm 1.8$, respectively; n.s.). Preparations of cortical and medullary membrane fractions were performed as described.[60] Total protein concentration was measured using a protein assay reagent kit (BCA; Pierce, Rockford, IL, USA).

Electrophoresis and SDS-polyacrylamide gel electrophoresis

SDS gel electrophoresis was performed on 6–10% gradient polyacrylamide gels. To confirm equal loading of protein, an initial gel was stained with Coomassie blue. After electrophoresis, the proteins were transferred to nitrocellulose membranes and stained with 0.1% Ponceau red. After incubation with blocking reagent, membranes were probed with primary antibodies and then exposed to horseradish peroxidase-conjugated secondary antibodies (DAKO, Hamburg, Germany). Immunoreactive bands were visualized using an enhanced chemiluminescence kit and exposure to X-ray films (Amersham Pharmacia, Buckinghamshire, UK). Films were analyzed using BIO-PROFIL Bio-1D image software (Vilber Lourmat, Germany). Finally, all data were corrected for β-actin expression.

Antibodies

For immunohistochemistry and immunoblotting, we employed well-characterized antibodies to the following proteins: C5b-9 membrane attack complex (gift from S. Shankland, Washington, WA, USA); AQP1 (BD Transduction laboratories, San Jose, CA, USA); NaPi-IIa (gift from J. Biber, Zurich, Switzerland); NHE3 (Biotrend, Cologne, Germany); megalin (raised against a C-terminal peptide sequence); villin (gift from D. Drenckhahn, Würzburg, Germany); β-actin (Sigma Aldrich, Munich, Germany); NKCC2 and NCC (both gifts from D. Ellison, Portland, OR, USA); α-, β-, and γ-subunits of ENaC (gift from B. Rossier (Lausanne, Switzerland)) and sera produced against N-terminal GST protein of α-subunit and C-terminal GST proteins of β- and γ-subunits of ENaC; αNKA and βNKA (Upstate Biotechnology, Lake Placid, NY, USA); AQP2 (Santa Cruz Biotechnology, Santa Cruz, CA, USA); renin (gift from A. Kurtz, Regensburg, Germany); α-tubulin (Sigma Aldrich); and 11βHSD-2 (Chemicon, Temecula, NM, USA). For f-actin staining, Alexa 488-phalloidin (Invitrogen, Carlsbad, CA, USA) was used.

Immunohistochemistry

Immunohistochemical staining was performed on cryostat or paraffin sections and on cells grown on glass cover slips. Initially, sections were blocked and incubated with the respective primary antibody followed by incubation with suitable horseradish peroxidase (DAKO) or cy-2- or cy-3-coupled secondary antibodies (Dianova, Hamburg, Germany). In double-labeling experiments, the primary antibodies were administered consecutively. Nuclei were stained blue with 4′,6-diamino-2-phenylindole. Counterstained sections and cells were analyzed using Leica DMRB microscope or multilaser confocal scanning microscope (TCS SP-2; Leica Microsystems, Bernsheim, Germany).

Periodic acid Schiff, Sudan III, and filipin staining

For histochemical detection of glycoproteins and lipid classes, 4-μm thick cryostat or paraffin sections were stained with periodic acid Schiff reagent or Sudan III. For filipin staining, cryostat sections were blocked with 0.5% bovine serum albumin or 1% goat serum in PBS and incubated for 2 h with 0.005% filipin complex dissolved in dimethyl sulfoxide (Sigma Aldrich). As a negative control, an equivalent concentration of DMSO alone was used.

Analysis of membrane lipid composition

To evaluate membrane lipid composition, BBM and medullary membrane preparations were methanol extracted according to the Bligh–Dyer method. The absolute amounts of lipids were then determined by reverse-phase high-performance liquid chromatography, separating free cholesterol and the major cholesterol esters (cholesteryl arachidonate, cholesteryl linoleate, cholesterol oleate, and cholesteryl stearate).[61]

In situ hybridization

The mRNA expression of renin was explored by *in situ* hybridization using digoxigenin-labeled riboprobes (Roche, Grenzach-Wyhlen, Germany). Sense and antisense probes were generated by *in vitro* transcription of 300 bp fragment of the corresponding cDNA. *In situ* hybridization was performed on paraffin sections according to an established protocol.[60]

Renal and plasma renin contents

To estimate tissue activity of the renin angiotensin system, histochemical signals were semiquantitatively evaluated. Alterations in renin transcripts and protein abundance were registered. The mean number of renin-positive sites at the juxtaglomerular apparatus and the upstream locations in preglomerular vessels was determined within an area of approximately 100 glomeruli.[62] Both the amount of renin mRNA and immunoreactive renin-containing afferent arterioles was quantified. PRA was measured with a commercial radioimmunoassay kit (Gammacoat; DiaSorin, Stillwater, MN, USA). One microliter of plasma was mixed on ice with 24 μl of maleate buffer containing EDTA, neomycin sulfate, and phenylmethanesulfonylfluoride. To determine background angiotensin I levels, 12 μl of this mix was removed and kept frozen until assaying. The remaining aliquot was incubated with angiotensinogen for 1 h at 37°C. Generated angiotensin I was measured by radioimmunoassay using standards and reagents provided by the manufacturer. In each assay, angiotensin I levels determined in the non-incubated plasma aliquot were subtracted (Beckman Multi Counter, Fullerton, CA, USA).

Plasma vasopressin concentrations

Plasma arg^8-vasopressin concentrations were determined by enzyme immunoassay according to the manufacturer's protocol (Assay Designs, Ann Arbor, MI, USA). All assays were run in duplicate. Recombinant arg^8-vasopressin provided by the manufacturer was used to establish a standard curve for calculation of sample arg^8-vasopressin concentrations. Sample absorption was determined at 405 nm with correction at 570 nm (uQuant; Biotek-Instruments, Winooski, VT, USA).

Presentation of data and statistical analysis

Quantitative data are presented as means ± s.e. For statistical comparison, the Mann–Whitney rank-sum test was employed. *P*-values less than 0.05 were considered statistically significant.

DISCLOSURE

All the authors declared no competing interests.

ACKNOWLEDGMENTS

We gratefully acknowledge the support from the Deutsche Forschungsgemeinschaft (FOR 667; HP, SB, and FT). We thank Kerstin Riskwosky (FOR 667, Berlin) for technical expertise, and Hermann Pavenstädt and Walter Zidek (Departments of Nephrology in Münster and Berlin, respectively, Germany) for helpful advice.

SUPPLEMENTARY MATERIAL

Table S1. Summary of immunoblotting results of Na^+, K^+-ATPase (NKA), and full-length and cleavage products of epithelial Na^+ channel (ENaC) α- and γ-subunits on days 2 and 4.

Figure S1. Semiquantitative immunoblotting of α-subunit of Na^+, K^+-ATPase (NKA), and α- and γ-subunits of the epithelial Na^+-channel (ENaC) from whole kidney membrane fractions on the day 2 and 4.

Supplementary material is linked to the online version of the paper at http://www.nature.com/ki

REFERENCES

1. Abbate M, Zoja C, Remuzzi G. How does proteinuria cause progressive renal damage? *J Am Soc Nephrol* 2006; **17**: 2974–2984.
2. Gekle M. Renal tubule albumin transport. *Annu Rev Physiol* 2005; **67**: 573–594.
3. Theilig F, Kriz W, Jerichow T *et al.* Abrogation of protein uptake through megalin-deficient proximal tubules does not safeguard against tubulointerstitial injury. *J Am Soc Nephrol* 2007; **18**: 1824–1834.
4. Kriz W, Hähnel B, Hosser H *et al.* Pathways to recovery and loss of nephrons in anti-Thy-1 nephritis. *J Am Soc Nephrol* 2003; **14**: 1904–1926.
5. Kuusniemi AM, Lapatto R, Holmberg C *et al.* Kidneys with heavy proteinuria show fibrosis, inflammation, and oxidative stress, but no tubular phenotypic change. *Kidney Int* 2005; **68**: 121–132.
6. Orth SR, Ritz E. [Nephrotic syndrome]. *Internist (Berl)* 1998; **39**: 1246–1252.
7. Doucet A, Favre G, Deschenes G. Molecular mechanism of edema formation in nephrotic syndrome therapeutic implications. *Pediatr Nephrol* 2007; **22**: 1983–1990.
8. Epstein AA. Concerning the causation of edema in chronic parenchymatous nephritis; method for its alleviation. *Am J Med* 1952; **13**: 556–561.
9. Kim SW, Wang W, Nielsen J *et al.* Increased expression and apical targeting of renal ENaC subunits in puromycin aminonucleoside-induced nephrotic syndrome in rats. *Am J Physiol Renal Physiol* 2004; **286**: F922–F935.
10. Lourdel S, Loffing J, Favre G *et al.* Hyperaldosteronemia and activation of the epithelial sodium channel are not required for sodium retention in puromycin-induced nephrosis. *J Am Soc Nephrol* 2005; **16**: 3642–3650.
11. Audigé A, Yu ZR, Frey BM *et al.* Epithelial sodium channel (ENaC) subunit mRNA and protein expression in rats with puromycin aminonucleoside-induced nephrotic syndrome. *Clin Sci (Lond)* 2003; **104**: 389–395.
12. Hricik DE, Chung-Park M, Sedor JR. Glomerulonephritis. *N Engl J Med* 1998; **339**: 888–899.
13. Besse-Eschmann V, Klisic J, Nief V *et al.* Regulation of the proximal tubular sodium/proton exchanger NHE3 in rats with puromycin aminonucleoside (PAN)-induced nephrotic syndrome. *J Am Soc Nephrol* 2002; **13**: 2199–2206.
14. Deschenes G, Doucet A. Collecting duct (Na+/K+)-ATPase activity is correlated with urinary sodium excretion in rat nephrotic syndromes. *J Am Soc Nephrol* 2000; **11**: 604–615.
15. Yang L, Leong PK, Chen JO *et al.* Acute hypertension provokes internalization of proximal tubule NHE3 without inhibition of transport activity. *Am J Physiol Renal Physiol* 2002; **282**: F730–F740.
16. Lötscher M, Kaissling B, Biber J *et al.* Role of microtubules in the rapid regulation of renal phosphate transport in response to acute alterations in dietary phosphate content. *J Clin Invest* 1997; **99**: 1302–1312.
17. Sabolic I, Ljubojevic M, Herak-Kramberger CM *et al.* Cd-MT causes endocytosis of brush-border transporters in rat renal proximal tubules. *Am J Physiol Renal Physiol* 2002; **283**: F1389–F1402.
18. Anders HJ, Vielhauer V, Schlöndorff D. Chemokines and chemokine receptors are involved in the resolution or progression of renal disease. *Kidney Int* 2003; **63**: 401–415.
19. Peters H, Wang Y, Loof T *et al.* Expression and activity of soluble guanylate cyclase in injury and repair of anti-thy1 glomerulonephritis. *Kidney Int* 2004; **66**: 2224–2236.
20. Tian YC, Fraser D, Attisano L *et al.* TGF-beta1-mediated alterations of renal proximal tubular epithelial cell phenotype. *Am J Physiol Renal Physiol* 2003; **285**: F130–F142.
21. Zager RA, Johnson AC, Hanson SY *et al.* Acute tubular injury causes dysregulation of cellular cholesterol transport proteins. *Am J Pathol* 2003; **163**: 313–320.
22. Johnson AC, Yabu JM, Hanson S *et al.* Experimental glomerulopathy alters renal cortical cholesterol, SR-B1, ABCA1, and HMG CoA reductase expression. *Am J Pathol* 2003; **162**: 283–291.
23. Murtazina R, Kovbasnjuk O, Donowitz M *et al.* Na+/H+ exchanger NHE3 activity and trafficking are lipid Raft-dependent. *J Biol Chem* 2006; **281**: 17845–17855.
24. Levi M, Baird BM, Wilson PV. Cholesterol modulates rat renal brush border membrane phosphate transport. *J Clin Invest* 1990; **85**: 231–237.
25. Ichikawa I, Rennke HG, Hoyer JR *et al.* Role for intrarenal mechanisms in the impaired salt excretion of experimental nephrotic syndrome. *J Clin Invest* 1983; **71**: 91–103.
26. Bernard DB, Alexander EA, Couser WG *et al.* Renal sodium retention during volume expansion in experimental nephrotic syndrome. *Kidney Int* 1978; **14**: 478–485.
27. Kim SW, de Seigneux S, Sassen MC *et al.* Increased apical targeting of renal ENaC subunits and decreased expression of 11betaHSD2 in HgCl2-induced nephrotic syndrome in rats. *Am J Physiol Renal Physiol* 2006; **290**: F674–F687.
28. Deschenes G, Wittner M, Stefano A *et al.* Collecting duct is a site of sodium retention in PAN nephrosis. A rationale for amiloride therapy. *J Am Soc Nephrol* 2001; **12**: 598–601.
29. Hughey RP, Carattino MD, Kleyman TR. Role of proteolysis in the activation of epithelial sodium channels. *Curr Opin Nephrol Hypertens* 2007; **16**: 444–450.
30. Svenningsen P, Jensen BL, Skøtt O. Plasmin stimulates the epithelial sodium channel via interaction with prostasin. *J Am Soc Nephrol* 2007; **18**: 38A.
31. Bengrine A, Li J, Hamm LL *et al.* Indirect activation of the epithelial Na+ channel by trypsin. *J Biol Chem* 2007; **282**: 26884–26896.
32. Bagchus WM, Hoedemaeker PJ, Rozing J *et al.* Glomerulonephritis induced by monoclonal anti-Thy 1.1 antibodies. A sequential histological and ultrastructural study in the rat. *Lab Invest* 1986; **55**: 680–687.
33. Burg M, Ostendorf T, Mooney A *et al.* Treatment of experimental mesangioproliferative glomerulonephritis with non-anticoagulant heparin: therapeutic efficacy and safety. *Lab Invest* 1997; **76**: 505–516.
34. Liebler S, Uberschar B, Kubert H *et al.* The renal retinoid system: time-dependent activation in experimental glomerulonephritis. *Am J Physiol Renal Physiol* 2004; **286**: F458–F465.
35. Dechow C, Morath C, Peters J *et al.* Effects of all-trans retinoic acid on renin–angiotensin system in rats with experimental nephritis. *Am J Physiol Renal Physiol* 2001; **281**: F909–F919.
36. Leong PK, Devillez A, Sandberg MB *et al.* Effects of ACE inhibition on proximal tubule sodium transport. *Am J Physiol Renal Physiol* 2006; **290**: F854–F863.
37. Ma T, Yang B, Gillespie A *et al.* Severely impaired urinary concentrating ability in transgenic mice lacking aquaporin-1 water channels. *J Biol Chem* 1998; **273**: 4296–4299.
38. Schnermann J, Chou CL, Ma T *et al.* Defective proximal tubular fluid reabsorption in transgenic aquaporin-1 null mice. *Proc Natl Acad Sci USA* 1998; **95**: 9660–9664.
39. Liang K, Vaziri ND. Gene expression of lipoprotein lipase in experimental nephrosis. *J Lab Clin Med* 1997; **130**: 387–394.
40. Kamijo Y, Hora K, Kono K *et al.* PPARalpha protects proximal tubular cells from acute fatty acid toxicity. *J Am Soc Nephrol* 2007; **18**: 3089–3100.
41. Inoue M, Digman MA, Cheng M *et al.* Partitioning of NaPi cotransporter in cholesterol-, sphingomyelin-, and glycosphingolipid-enriched membrane domains modulates NaPi protein diffusion, clustering, and activity. *J Biol Chem* 2004; **279**: 49160–49171.
42. Crane JM, Verkman AS. Long-range nonanomalous diffusion of quantum dot-labeled aquaporin-1 water channels in the cell plasma membrane. *Biophys J* 2008; **94**: 702–713.
43. Welker P, Geist B, Frühauf JH *et al.* Role of lipid rafts in membrane delivery of renal epithelial Na+-K+-ATPase, thick ascending limb. *Am J Physiol Regul Integr Comp Physiol* 2007; **292**: R1328–R1337.

44. Welker P, Böhlick A, Mutig K *et al.* Renal Na-K-Cl cotransporter activity and vasopressin-induced trafficking are lipid raft-dependent. *Am J Physiol* 2008; **295**: F559–F567.
45. Hill WG, Butterworth MB, Wang H *et al.* The epithelial sodium channel (ENaC) traffics to apical membrane in lipid rafts in mouse cortical collecting duct cells. *J Biol Chem* 2007; **282**: 37402–37411.
46. Theilig F, Kastner C, Sendeski M *et al.* Protein uptake interferes with proximal tubular transport. *J Am Soc Nephrol* 2007; **18**: 116A.
47. Teng Y, Zeisberg M, Kalluri R. Transcriptional regulation of epithelial–mesenchymal transition. *J Clin Invest* 2007; **117**: 304–306.
48. Baus M, Medjugorac-Popovski M, Brown D *et al.* In colchicine-treated rats, cellular distribution of AQP-1 in convoluted and straight proximal tubule segments is differently affected. *Pflugers Arch* 2000; **439**: 321–330.
49. Lang F, Klingel K, Wagner CA *et al.* Deranged transcriptional regulation of cell-volume-sensitive kinase hSGK in diabetic nephropathy. *Proc Natl Acad Sci USA* 2000; **97**: 8157–8162.
50. Fernandez-Llama P, Andrews P, Ecelbarger CA *et al.* Concentrating defect in experimental nephrotic syndrone: altered expression of aquaporins and thick ascending limb Na+ transporters. *Kidney Int* 1998; **54**: 170–179.
51. Féraille E, Mordasini D, Gonin S *et al.* Mechanism of control of Na,K-ATPase in principal cells of the mammalian collecting duct. *Ann NY Acad Sci* 2003; **986**: 570–578.
52. Bistrup C, Thiesson HC, Jensen BL *et al.* Reduced activity of 11beta-hydroxysteroid dehydrogenase type 2 is not responsible for sodium retention in nephrotic rats. *Acta Physiol Scand* 2005; **184**: 161–169.
53. Blot-Chabaud M, Jaisser F, Gingold M *et al.* Na+-K+-ATPase-dependent sodium flux in cortical collecting tubule. *Am J Physiol Renal Physiol* 1988; **255**: F605–F613.
54. Vallet V, Chraibi A, Gaeggeler HP *et al.* An epithelial serine protease activates the amiloride-sensitive sodium channel. *Nature* 1997; **389**: 607–610.
55. Harris M, Firsov D, Vuagniaux G *et al.* A novel neutrophil elastase inhibitor prevents elastase activation and surface cleavage of the epithelial sodium channel expressed in *Xenopus laevis* oocytes. *J Biol Chem* 2007; **282**: 58–64.
56. Diakov A, Bera K, Mokrushina M *et al.* Cleavage in the {gamma}-subunit of the epithelial sodium channel (ENaC) plays an important role in the proteolytic activation of near-silent channels. *J Physiol* 2008; **586**(Part 19): 4587–4608.
57. Ergonul Z, Frindt G, Palmer LG. Regulation of maturation and processing of ENaC subunits in the rat kidney. *Am J Physiol Renal Physiol* 2006; **291**: F683–F693.
58. Stahl R, Thaiss F, Kahf S *et al.* Immune-mediated mesangial cell injury—Biosynthesis and function of prostanoids. *Kidney Int* 1990; **38**: 273–281.
59. Bachmann S, Schlichting U, Geist B *et al.* Kidney-specific inactivation of the megalin gene impairs trafficking of renal inorganic sodium phosphate cotransporter (NaPi-IIa). *J Am Soc Nephrol* 2004; **15**: 892–900.
60. Theilig F, Debiec H, Nafz B *et al.* Renal cortical regulation of COX-1 and functionally related products in early renovascular hypertension (rat). *Am J Physiol Renal Physiol* 2006; **291**: F987–F994.
61. Walther M, Wiesner R, Kuhn H. Investigations into calcium-dependent membrane association of 15-lipoxygenase-1. Mechanistic roles of surface-exposed hydrophobic amino acids and calcium. *J Biol Chem* 2004; **279**: 3717–3725.
62. Bosse HM, Böhm R, Resch S *et al.* Parallel regulation of constitutive NO synthase and renin at JGA of rat kidney under various stimuli. *Am J Physiol Renal Physiol* 1995; **269**: F793–F805.